

iDISCO: A Simple, Rapid Method to Immunolabel Large Tissue Samples for Volume Imaging

Nicolas Renier,^{1,3} Zhuhao Wu,^{1,3} David J. Simon,¹ Jing Yang,¹ Pablo Ariel,² and Marc Tessier-Lavigne^{1,*}

¹Laboratory of Brain Development and Repair

²Bio-Imaging Resource Center

The Rockefeller University, 1230 York Avenue, New York, NY 10065, USA

³Co-first author

*Correspondence: marctl@rockefeller.edu

<http://dx.doi.org/10.1016/j.cell.2014.10.010>

SUMMARY

The visualization of molecularly labeled structures within large intact tissues in three dimensions is an area of intense focus. We describe a simple, rapid, and inexpensive method, iDISCO, that permits whole-mount immunolabeling with volume imaging of large cleared samples ranging from perinatal mouse embryos to adult organs, such as brains or kidneys. iDISCO is modeled on classical histology techniques, facilitating translation of section staining assays to intact tissues, as evidenced by compatibility with 28 antibodies to both endogenous antigens and transgenic reporters like GFP. When applied to degenerating neurons, iDISCO revealed unexpected variability in number of apoptotic neurons within individual sensory ganglia despite tight control of total number in all ganglia. It also permitted imaging of single degenerating axons in adult brain and the first visualization of cleaved Caspase-3 in degenerating embryonic sensory axons *in vivo*, even single axons. iDISCO enables facile volume imaging of immunolabeled structures in complex tissues.

INTRODUCTION

Immunolabeling is a central technique in many areas of biological research and medical diagnosis, making it possible to reveal the morphology and molecular composition of biological samples. However, its application has been mostly restricted to thin preparations or small samples owing to the difficulty of labeling and observing deep structures in intact specimens. 3D imaging is particularly valuable when analyzing complex structures that are not contained within 2D planes, such as axonal tracts or the vasculature. Moreover, volume data sets allow more flexibility for analysis than tissue sections for quantitative studies of cell number counts or relative distance measurements.

It has been recognized for a century that biological specimens can be made optically transparent by methods that

reduce internal differences in refractive index within the tissue to reduce scatter, thus enabling visualization of deep structures (Spalteholz, 1914). Recently, there has been a resurgence of interest in optimizing methods for volume imaging of molecularly labeled structures in large, cleared tissue samples, leading to the development of several important new clearing methods: ScaleA2 (Hama et al., 2011), 3DISCO (Ertürk et al., 2012a, 2012b, 2014), ClearT2 (Kuwajima et al., 2013), SeeDB (Ke et al., 2013), CLARITY (Chung et al., 2013; Tomer et al., 2014; Yang et al., 2014), and CUBIC (Susaki et al., 2014). These methods were mostly developed with an eye to preserving endogenous fluorescence of proteins such as GFP, YFP and mCherry expressed from transgenes. However, the steps used to achieve this in some cases constrain their versatility for rapid and robust immunolabeling. Several use aqueous solutions to preserve fluorescence, but this makes optical clearing slow for large tissues (2–6 weeks) and can hinder transparency for subsequent imaging; as well, some use highly denaturing agents (e.g., urea or SDS), to which some epitopes recognized by antibodies of interest may be sensitive, and some are difficult to implement and/or to scale (Table S1 available online).

In this study, we focused on establishing a simple, rapid, robust, scalable, and inexpensive method for whole-mount immunolabeling of deep tissue structures with volume imaging. We deemed the preservation of endogenous fluorescence of proteins like GFP to be valuable but not absolutely essential, because visualization of such proteins can also be achieved independently by immunolabeling them. We first systematically tested and modified existing whole-mount immunolabeling methods to achieve the best signal-to-noise ratio and deepest tissue penetration in a reasonable time frame in tissues ranging from large mouse embryos to adult mouse brains and other complex organs. We also evaluated the recently published clearing methods for their ability to support robust and rapid immunolabeling of a range of antigens. Table S1 lists strengths and limitations of each method for that purpose, as assessed in our hands. That analysis led us to focus on 3DISCO (3D imaging of solvent-cleared organs) (Ertürk et al., 2012a) because it is rapid, simple, and provides excellent clearing that is compatible with immunolabeling (Table S1).

Through this comprehensive analysis, we found that several modifications of existing whole-mount immunolabeling methods, when combined with 3DISCO clearing, create a platform that provides robust and reliable labeling of deep structures not just in large embryonic but also in dense adult tissues. We term this method immunolabeling-enabled three-dimensional imaging of solvent-cleared organs (iDISCO). Its strengths include the following.

- It enables deep antibody diffusion in tissues in whole embryos, even those as large as embryonic day 18.5 (E18.5), as well as in dense complex adult organs, including the brain and kidney.
- It is designed to be simple to implement and was modeled after traditional histology techniques, so all reagents for sample processing are common and inexpensive, and no special lab equipment is required.
- It has a relatively fast turnover because 3DISCO clearing takes only a day, compared to weeks for other methods with similar clearing performance (Table S1). Thus, multiple rounds of sequential analysis can be done in a reasonable time frame, as samples can be harvested, immunolabeled and cleared in 8–18 days depending on size (Table S2).
- Whereas some other clearing platforms cause samples to be unstable in the index matching solution, necessitating prompt imaging and storage in a different solution, iDISCO uses Alexa Fluor dyes, which can be imaged repeatedly with very low photobleaching and are stable for many months in the index matching solution at room temperature. The immunolabeling patterns are also fixed in the sample, with no diffusion over time.
- It is compatible with labeling methods relying on click-chemistry, as well as with some but not all histochemical dyes (e.g., dyes of the TO-PRO family of nuclear DNA stains).
- Importantly, if an antibody provides a good signal and low background when used in immunohistochemistry (IHC) on tissue sections, our experience indicates it has a good chance of working with iDISCO. Indeed, we tested 28 antibodies that work well in IHC and all worked successfully with iDISCO (Table S3).

Together with light-sheet microscopy (Dodd et al., 2007), these features make iDISCO a versatile, reliable, and consistent analytic platform and one that is easy to scale to large numbers of samples, potentially in the hundreds. We illustrate the application of the method to detect a variety of antigens (some sparse, some widely expressed) in numerous embryonic and adult neural and nonneural structures (including kidney, muscle, stomach, and the vasculature), to visualize proliferating cells and axonal projections, to visualize a reporter of neuronal activity (*c-fos*), and to address some outstanding questions in neural degeneration.

RESULTS

Whole-Mount Immunolabeling of Large Samples

Various whole-mount immunolabeling protocols have been developed to visualize marker expression in small specimens

such as young mouse embryos (generally up to E12.5), *Drosophila* larvae and brains, or mammalian—including human—brain slices up to 1 mm in thickness. We tested and combined some of these approaches, including the use of nonionic detergents and rounds of organic solvent-based dehydration-rehydration to remove membrane lipids for permeabilization of larger samples, as well as bleaching with hydrogen peroxide to reduce tissue autofluorescence. We found that combining glycine and heparin treatment to reduce immunolabeling background gave excellent results for whole mouse embryos up to stage E18.5, as well as whole adult mouse brains, kidneys, and other organs. The use of methanol for tissue bleaching improved immunolabeling for most antibodies we tested (25 of 28) but also prevented antigen recognition by a few (3 of 28) (see below). To broaden the spectrum of applications, we developed two alternate immunolabeling protocols, one with nondenaturing conditions and the other involving mild denaturation with methanol. For each antibody tested, we assessed which protocol to use by comparing signal-to-noise ratios (Table S3). When compatible, we recommend using methanol treatment, especially in adult tissues, to maximally reduce tissue autofluorescence and improve antibody diffusion; the nondenaturing approach provides an alternative if needed that can still give excellent results in embryos and trimmed adult tissues.

Because tissue autofluorescence of large biological samples is strong in the blue-green spectrum, fluorophores in the red spectrum help reduce background and ones in the far-red spectrum are even better (see comparison in Figure S1). In this study, we use Alexa Fluor-647 (far-red spectrum) for most stainings shown. Exceptions are Alexa Fluor-488 for TrkA colabeling in Figure 6B, Alexa Fluor-568 for Aquaporin 2 colabeling in Figure 4A, TrkA colabeling in Figure 4C, E16.5 forearm TrkA labeling in Figure 2C, and cCasp3 labeling in Figure 6.

Finally, after immunolabeling the ideal clearing protocol should not only provide excellent clearing, but also be rapid, easy to implement, inexpensive, and compatible with a broad range of antigens. In assessing clearing methods according to these five criteria, we found 3DISCO to be the best for our purposes (Table S1). 3DISCO was developed as an improvement over the classical benzyl alcohol-benzyl benzoate (BABB) method to enable clearing of lipid-rich tissues such as myelinated tracts in the adult nervous system and was initially used to visualize vasculature labeled with a fluorescent lectin and GFP-labeled axons (Ertürk et al., 2012a, 2012b). In our hands, it provides clearing that is as good or better than that of other methods we tested, and it is also extremely rapid (1 day), inexpensive, and very easy to implement (Table S1). One limitation is that the organic solvent it uses rapidly quenches endogenously fluorescent proteins, necessitating prompt imaging if the purpose is to visualize such signals (Ertürk et al., 2014; Ke et al., 2013). However, while not initially combined with immunolabeling, the methods are fully compatible (Ertürk et al., 2014; A. Chédotal, personal communication; our observations), and, importantly, Alexa Fluor dyes are very stable at room temperature in the organic solvents it uses.

The iDISCO protocol combines the steps of sample preparation and immunolabeling with stable fluorophores outlined above, together with a slightly simplified 3DISCO procedure, to

permit volume imaging of labeled molecules and structures in large intact samples. It is detailed in [Data S2](#).

Application of iDISCO

We first illustrate the utility of iDISCO using FoxP2 immunolabeling on adult (4 months old) mouse brain, as this transcription factor, well-studied for its role in the specification of neural networks involved in vocalization ([Enard et al., 2009](#)), is widely expressed throughout the brain ([Ferland et al., 2003; Fujita and Sugihara, 2012](#)). For processing, the brainstem and cerebellum were left intact, but the forebrain was cut in two to reduce the time required for good clearing and antibody diffusion. After immunolabeling and clearing, the brain was imaged on a light-sheet microscope.

In the brainstem, we detected FoxP2 expression in the inferior olive (IO) (see [Table S4](#) for a list of all anatomical abbreviations used here) in a pattern that perfectly matches that observed in cryosections made at the same level ([Figure 1A; Movie S1](#)) and in previous studies ([Fujita and Sugihara, 2012](#)). Consistent with a previous report ([Hornig et al., 2009](#)), FoxP2-positive cells were also detected throughout the whole forebrain, notably in the striatum, the sixth cortical layer, and the thalamic medial geniculate nucleus (MGN), thus showing that the deepest structures (more than 2 mm deep) could be labeled in patterns matching known FoxP2 expression ([Figure 1A](#)). The signal-to-noise ratio and resolution were sufficiently high to enable automated counting of the total number of FoxP2 positive cells in the IO using Imaris software. In the sample shown, 26,839 cells were counted, consistent with numbers previously estimated from tissue sections, i.e., between 24,000 and 30,000, depending on mouse strain ([Frederic et al., 1992](#)).

Application to Axonal Projections

Visualizing axon tracts is another important application for volume imaging. We used an antibody against tyrosine hydroxylase (TH) to label dopaminergic neurons and their projections in E15.5 embryos and adult brains ([Figure 1B](#)), iDISCO made it possible to label the entire embryonic head without dissecting out the brain, making the TH-positive peripheral sensory axons in the head also visible ([Figure 1B; Movie S1](#)). Using software, we could also perform a “virtual” dissection of the brain to examine axons just within the brain, without surrounding tissues in the head ([Figure 1B; Movie S1](#)). In this preparation, it was possible to follow the mesotelencephalic pathway (MTP) from the midbrain nuclei to the developing forebrain. In P0 whole brain and in adult midbrain, individual neurons of the substantia nigra (SN) and ventral tegmental area (VTA), as well as their projections, can be visualized ([Figure 1B](#)).

We also visualized axons of sensory neurons with cell bodies located in the dorsal root ganglia (DRGs). These neurons send axons to both the CNS and the periphery. Each DRG contains several subtypes of sensory neurons specialized for different kinds of inputs. The expression of the neurotrophin receptors TrkA, TrkB, TrkC, and Ret can be used to label distinct subpopulations. TrkA labels mostly nociceptive inputs, whereas TrkB, TrkC, Ret, and tyrosine hydroxylase label different kinds of low threshold mechanosensory receptor (LTMR) neurons ([Abraira and Ginty, 2013](#)). We visualized each of these subpopulations

in whole embryos at E12.5 ([Figure 2A](#)). TrkA, TrkC, and tyrosine hydroxylase antibodies exclusively labeled neuronal structures, whereas TrkB and Ret additionally labeled nonneuronal structures. An antibody to parvalbumin also successfully labeled a subset of DRG neurons ([Table S3](#) and data not shown). TrkA-labeled embryos from E12.5 to E16.5 could be rapidly imaged whole at high resolution (heads were removed for E16.5 embryos) ([Figure 2B; Movie S2](#)). We clearly and reproducibly labeled both major and minor nerve branches and observed fine details in regions such as the whisker pad, tongue, and entire forelimbs ([Figure 2C](#)), as well as the fibers innervating the skin ([Figure 2D](#)). Tuj1, which labels all axons, showed denser labeling in the same region ([Figure 2C](#)).

Application to Visualizing Transgenic Reporters

While antibodies that work well on histological sections are readily compatible with iDISCO, many structures cannot be specifically labeled with available antibodies to endogenous molecular markers. However, widely available transgenic mouse collections are a valuable resource for neuroanatomical studies of specific structures. We set out to apply iDISCO in a classic reporter line paradigm by using the ChAT::cre ; Rosa26^{lox-stop-lox-tdTmato} floxed reporter line, in which a fluorescent reporter (tdTomato) is expressed under the control of the choline acetyl transferase (ChAT) promoter, to visualize cholinergic neurons and their projections. We labeled a young adult (1 month old) mouse forebrain cut sagittally in half. In this preparation, we could visualize the motor nuclei of the Vth and IIIrd cranial nerves, the fasciculus retroflexus, and many cholinergic interneurons in the cortex and the striatum ([Figure 3A; Movie S3](#)). We also verified that the procedure enables a high-resolution view of the neurites of the cholinergic interneurons. It was possible to image and reconstruct individual neurons because of the sparse expression of the ChAT::cre in the cortex and striatum ([Figure 3A; Movie S3](#)).

Various Thy1::GFP lines were developed as a modern alternative to Golgi staining to label excitatory projection neurons ([Feng et al., 2000](#)). Using an Abcam anti-GFP antibody ([Table S3](#)), we tested iDISCO on the Thy1::GFP-M line, which has the most sparse GFP expression of all reported Thy1 lines ([Feng et al., 2000](#)). As shown in [Figure 3B](#) and [Movie S3](#), this sparse expression simultaneously enables imaging of the entire pattern throughout the brain (at lower magnification) together with resolution of individual axons (at high magnification). We also tested two additional GFP antibodies, one from Aves that also gave very good results with the methanol treatment protocol, and another from Invitrogen that worked only in nonmethanol-treated samples (and that is therefore not recommended) ([Table S3](#) and data not shown).

Epitope tags such as LacZ, HA, and myc are also commonly used. We expect the method to work with any tag for which there is a good antibody that works well in IHC on sections. As an example, we tested the compatibility of iDISCO with the LacZ tag in a *Netrin-1* gene-trap line in which a β-galactosidase fusion is driven from the *Netrin-1* locus ([Serafini et al., 1996](#)). Using an antibody to β-galactosidase, high level expression was observed at the midline in the spinal cord and caudal brain as expected ([Serafini et al., 1996](#)), and lower levels could be observed in

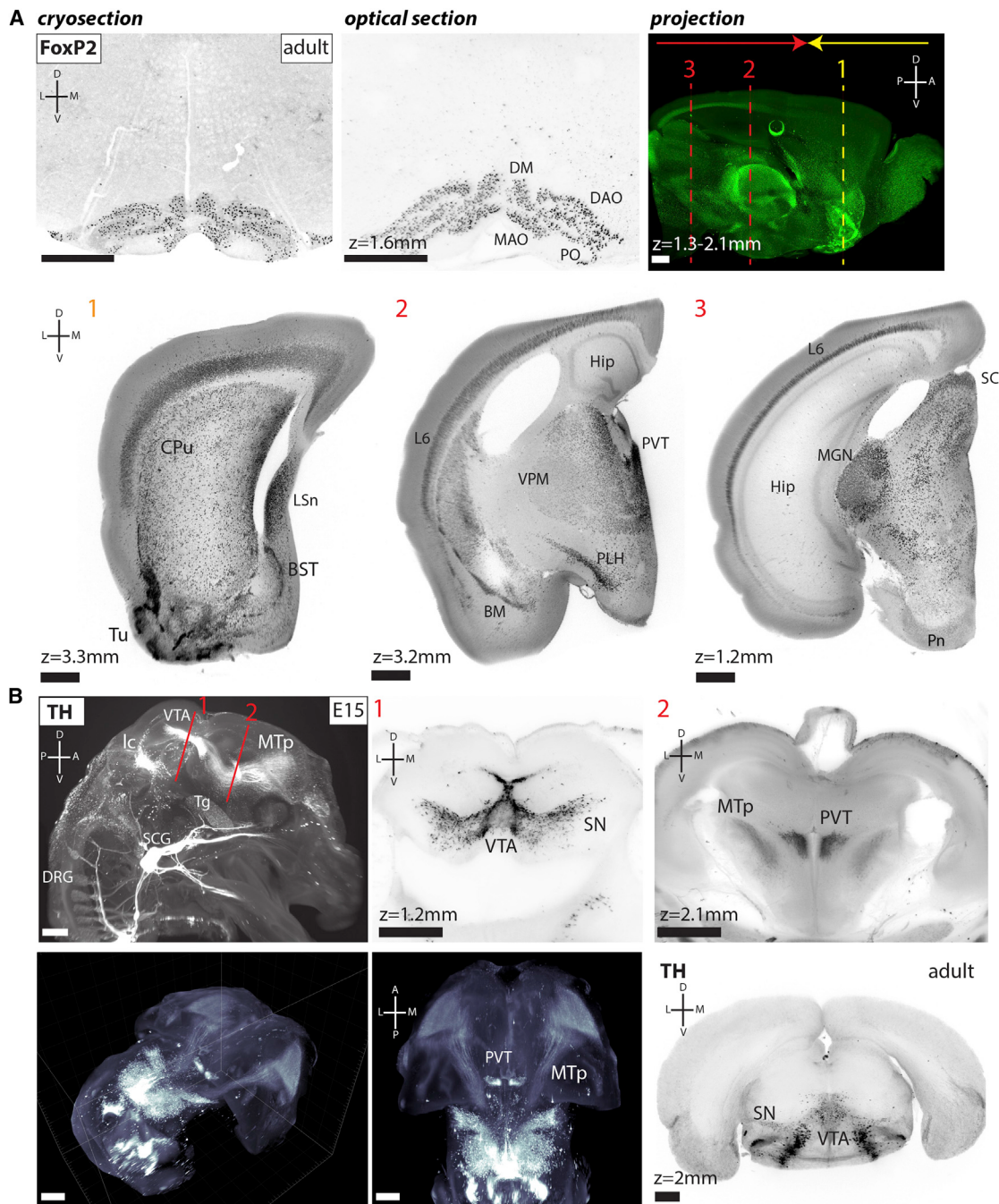
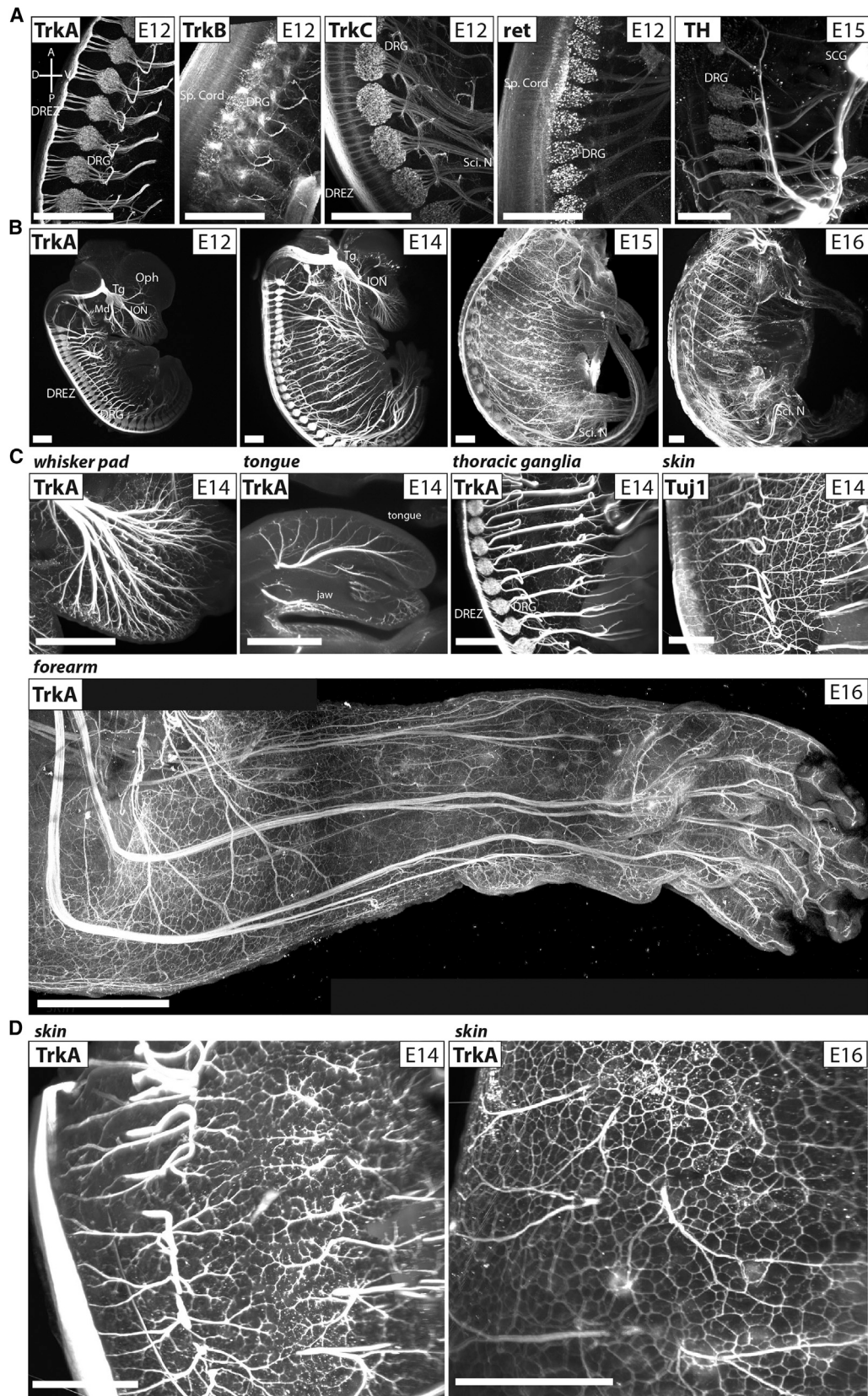


Figure 1. Whole-Mount Immunolabeling of Adult Brain and Entire Embryonic Head

(A) FoxP2 immunolabeling of a 4-month-old mouse brain. The coronal 35 μ m cryosection immunolabeled for FoxP2 at the level of the Inferior Olive, and the matching coronal optical plane (1.6 mm deep in the tissue) from a whole-mount-labeled caudal adult brain (cerebellum and hindbrain). Right: sagittal projection of an adult half-forebrain, showing FoxP2 labeling in the cortex, olfactory bulb, striatum, and thalamus. The brain was scanned in coronal orientation from both rostral and caudal ends. The scans met in the middle of the sample. Optical sections at the indicated levels from the same brain are shown below.

(B) Top tyrosine hydroxylase (TH) labeling of an E15.5 mouse embryo head showing optical sections through the midbrain and thalamus, and virtual dissections of the brain (bottom). Bottom: optical section of an adult (8 weeks old) mouse midbrain showing dopaminergic neurons of the midbrain. Anatomical abbreviations are listed in Table S4. Scale bars represent 500 μ m.

See also Figure S3, Tables S1, S2, S3, and S4, and Movie S1.



(legend on next page)

skin and various organs such as tongue, limbs, and heart (Figure 3C; Movie S3).

Application to Nonneuronal Tissues and Use of Widely Expressed Markers

We tested iDISCO on whole adult mouse kidneys, which are approximately the size of E14.5 mouse embryos. We could visualize and count all glomeruli in intact kidney by immunolabeling for nephrin (Figure 4A; Movie S4). To visualize the collecting ducts, we immunolabeled for Aquaporin 2 (Figure 4A; Movie S4). We noticed in initial experiments that the Aquaporin 2 antibodies did not penetrate the center of the sample. We reasoned that this might be due to the very high abundance of the protein in kidney, which could result in most IgG molecules being adsorbed on the superficial ducts. After estimating the coverage in the first attempts (~20%), we increased the concentration of the antibody 10-fold (from 1/200 to 1/20 dilution) and successfully labeled all collecting ducts in a whole kidney (see Figure S2).

General nuclear stains are a valuable tool to quickly label tissues and reveal their ultrastructure. We screened for nuclear DNA stains that could be compatible with iDISCO. Although Draq5 and Hoechst were not compatible, we found that cyanine-based dyes of the TO-PRO family of nuclear DNA stains worked well, which we used as a counterstain for Aquaporin 2 in adult kidney (Figure 4A; Movie S4). It should be noted that to be useful in resolving individual cells, general nuclear stains require high resolution imaging (Figure S3), which was beyond the resolution of the light-sheet microscope available to us and achieved here using confocal microscopy. We designed a 3D-printed imaging chamber to enable the use of confocal and two-photon microscopes (Figure S4; Data S1).

Imaging at higher resolution with confocal and/or two-photon microscopy also enabled us to use two widely expressed general markers, E-cadherin and β -catenin, to help identify different types of kidney tubules (Reginensi et al., 2013) (Figure 4A; Movie S4). Anti-laminin was also useful for that purpose, and because of its sparser labeling, could be imaged effectively with our light-sheet microscope (Movie S4). We also found that general markers of the extracellular matrix can also be used to visualize cellular architecture in other organs, including muscle (Figure 4B; Movie S4) and stomach (Movie S4).

To visualize vasculature, we used an antibody against PeCAM to immunolabel blood vessels, in combination with TrkA for sensory axons in E14.5 embryos (Figure 4C; Movie S4). As for Aquaporin 2, PeCAM-labeling required a high antibody concentration to achieve full coverage. The CNS as well as internal organs such as the heart (Figure 4C), kidney, and intestines, were well labeled. Although axons and vessels are well known

to be aligned in many tissues, in the face colabeling of the vasculature and main axonal tracts did not reveal a perfect overlap, especially in the case of the major branches of both systems (Figure 4C), consistent with a recent report (Oh and Gu, 2013).

Application to Cell Proliferation, Click Chemistry, and Phosphorylated Epitopes

Cell proliferation in developing or adult tissues can be visualized with a pulse of a synthetic nuclei acid like BrdU or EdU, which is detected using click chemistry. We tested the compatibility of EdU and the click chemistry reactions with iDISCO by giving a pulse of EdU to a pregnant dam at day 14 of gestation and harvesting embryos 1 hr later. Embryos were processed with the iDISCO protocol, and the click reaction was performed as directed. EdU incorporation could be visualized as expected in skin and proliferative regions after clearing (Figure 5A; Movie S5). In the brain, EdU incorporation was seen in the neurogenic regions, such as the subventricular zone, the third ventricle, the midbrain, the cerebellum, and the rhombic lips in the hindbrain.

Phosphohistone H3 (pHH3) is another commonly used marker to study cell proliferation. The labeling is sparse compared to EdU as pHH3 only labels cells in metaphase. We labeled intact E14 embryos with pHH3. Because of the sparse labeling, we could discriminate individual dividing cells in various brain regions at low magnification (Figure 5B; Movie S5). Virtual dissection of the lateral ventricle enabled a complete view of all dividing cells in the telencephalon (Movie S5).

Many other phosphorylated epitopes are also of interest for a variety of applications. We tested antibodies to two distinct phosphorylated epitopes on cJun for their ability to detect cJun phosphorylation in DRG sensory neurons triggered by sciatic nerve transection, and both worked well (Table S3 and data not shown).

Application to Neuronal Activity

Recent neuronal activity can be probed postmortem by the neuronal expression of immediate early genes (IEGs) (Goelet et al., 1986). Among the IEGs, c-fos expression has been shown to label recently active neurons in many systems where its expression is usually triggered about 30 min after a stimulus. In the spinal cord, c-fos expression can be induced in dorsal horn interneurons after a painful stimulus of the hind paw (Hunt et al., 1987). We tested the compatibility of c-fos immunolabeling with iDISCO in lumbar spinal cord. The left hind paws of anesthetized adult mice were dipped in a 52°C water bath and the mice were left to recover for 2 hr. C-fos immunolabeling was observed in 3D unilaterally in the left dorsal horn at the levels of the roots of

Figure 2. Whole-Mount Imaging of the Embryonic Peripheral Sensory Nervous System

- (A) E12.5 embryos labeled for TrkA, TrkB, TrkC, and ret, and E15 embryo labeled for tyrosine hydroxylase. Sagittal maximum projections at the level of the thoracic (TrkA and TrkB), lumbar (TrkC), or cervical (ret and TH) DRGs.
 - (B) Half projections of whole embryos labeled for TrkA.
 - (C) Details of the TrkA innervation at E14.5 in the whisker pad, tongue, and thoracic DRGs, and Tuj1-labeled innervation in the flank skin. E16.5 forearm labeled with TrkA and imaged with a two-photon microscope.
 - (D) Partial projections of the flank region in E14.5 and E16.5 whole embryos labeled for TrkA showing skin innervation. Anatomical abbreviations are listed in Table S4. Scale bars represent 500 μ m.
- See also Figures S1, S3, and S4, Tables S1, S2, S3, and S4, and Movie S2.

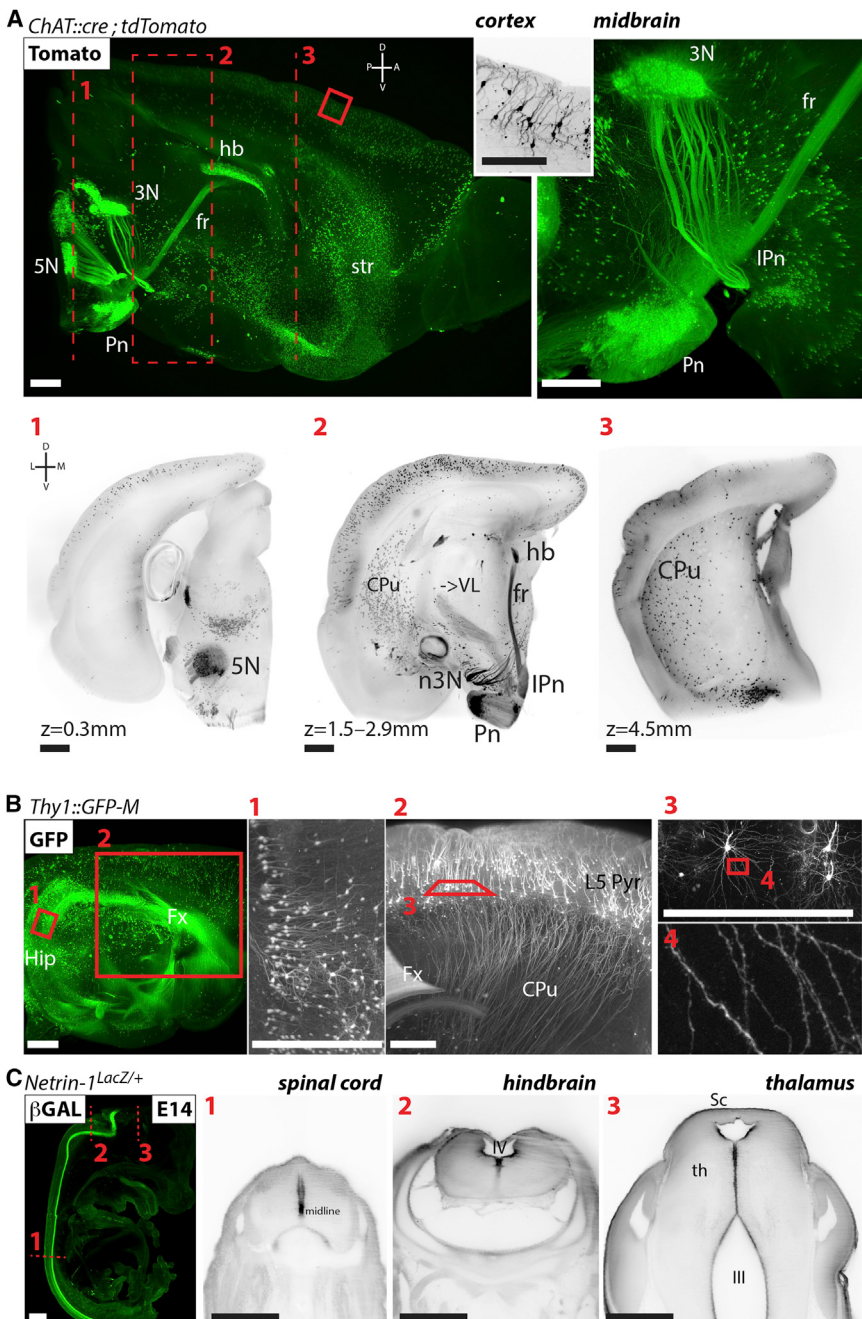


Figure 3. Whole-Mount Immunolabeling of Transgenic Reporter Lines

(A) Projection of a whole-mount RFP immunolabeling of a 1-month-old mouse half forebrain from a *ChAT::cre ; Rosa26^{lsl-tdTomato}* reporter line, showing details of the midbrain, cortex and optical sections at different levels.

(B) Whole-mount GFP immunolabeling of a 1-month-old mouse half forebrain from a *Thy1::GFP-M* line. Insets: details of the hippocampus, striatum, and cortical pyramidal neurons.

(C) Whole-mount β -galactosidase immunolabeling of an E14 *Netrin-1LacZ/+* embryo. Sagittal optical section at the level of the spinal cord and transverse optical sections at the levels of the spinal cord, hindbrain, and thalamus. Anatomical abbreviations are listed in Table S4. Scale bars represent 500 μ m.

See also Figure S3, Tables S1, S2, S3, and S4, and Movie S3.

sults from proteolytic cleavage by upstream caspases. Using iDISCO, we visualized cCasp3 in many DRG neuron cell bodies (Figure 6A); labeling was specific, as it was completely abolished in embryos lacking Casp3. It was also largely abolished in sensory neurons in mice mutant for *Bax*, which is upstream of Casp3, but was still present in non-neuronal cells, consistent with a known redundancy of *Bax* and its relative *Bak* in some tissues (Lindsten et al., 2000). Interestingly, a few cCasp3 positive neurons remained in some DRGs in *Bax*^{-/-} embryos, suggesting redundancy with *Bak* in subsets of sensory neurons as well (Middleton and Davies, 2001). We also visualized cleaved Caspase 9 (cCasp9) with iDISCO in subsets of sensory neurons, although the antibody only worked without methanol pretreatment and yielded a weaker signal (Table S3 and data not shown).

Genetic and other evidence implies that Casp3 is also required within sensory axons for degeneration in vitro and axon

the L4 and L5 DRGs (Figure 5C; Movie S6). We also observed deeper c-fos-positive interneurons and motoneurons, showing that antibody penetration was not limited to the superficial layers in this heavily myelinated tissue.

Application to Apoptosis and Neurodegeneration

Naturally occurring apoptotic cell death during development is critical for determining the final number of sensory neurons in adult DRGs (Deckwerth et al., 1996; Sun et al., 2003; White et al., 1998). This process can be studied using antibodies that recognize a neo-epitope within Caspase-3 (Casp3) that re-

pruning in vivo (Simon et al., 2012), but detection of cCasp3 in axons in vivo during normal development has remained elusive. Using a more sensitive antibody to cCasp3 (Table S3) in combination with iDISCO, we were able to document for the first time the presence of cCasp3 in sensory axons from the DRG and trigeminal ganglion during developmental degeneration in vivo (Figure 6B). In *Bax*^{-/-} embryos, where cCasp3+ neurons are rare (see above), staining was sufficiently sparse that cCasp3 could be observed with single axon resolution (Figure 6A, inset). Interestingly, we did not observe enrichment of cCasp3 at axonal branch points, which is different from what has been reported

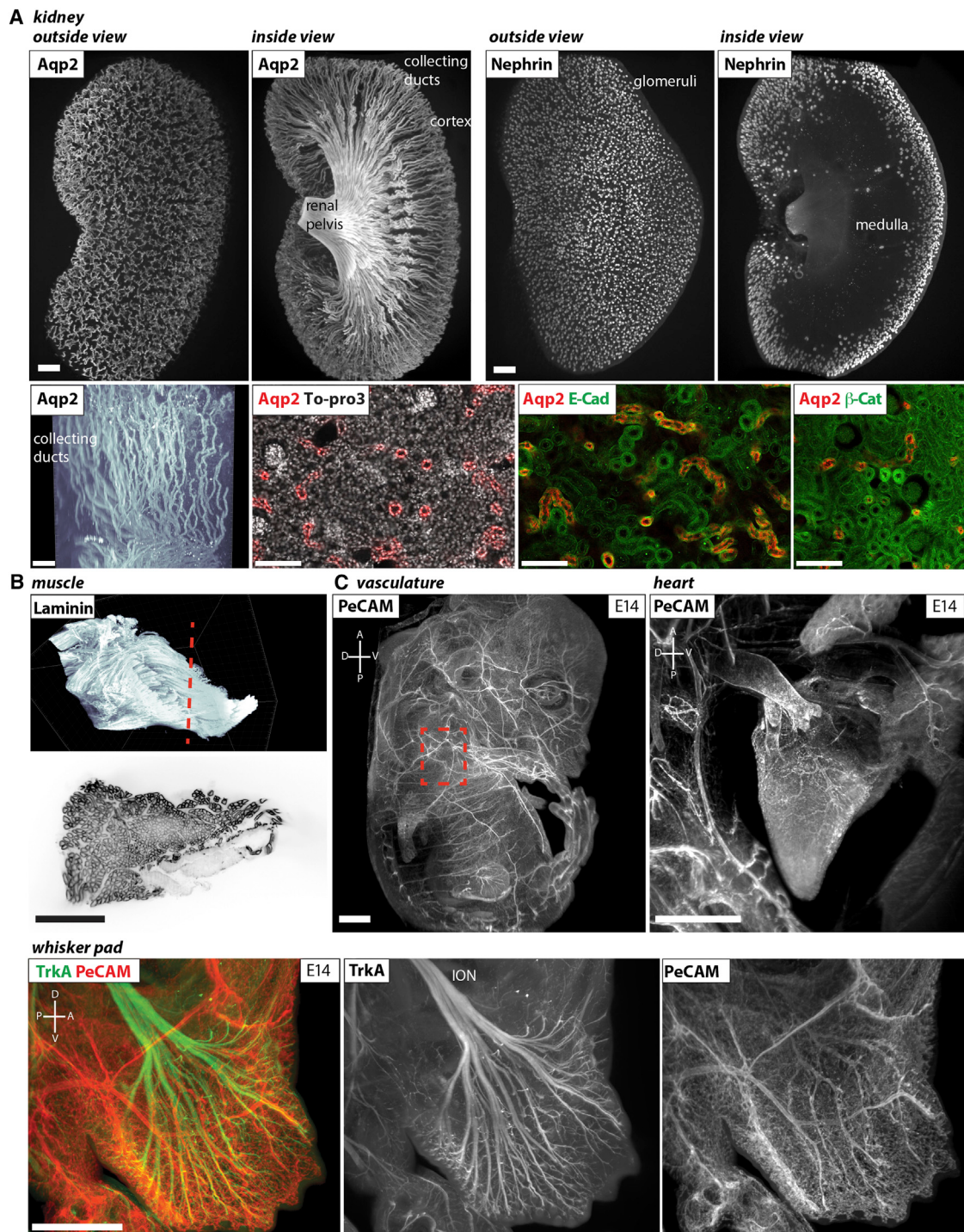


Figure 4. Application to Adult Kidney and Muscle and Embryonic Vasculature

(A) Upper row: Aquaporin2 labeling in adult mouse half-kidneys (labeling collecting ducts), and Nephrin in mouse whole kidneys (labeling glomeruli). Lower row: higher magnification optical sections of Aquaporin2 colabeled with TO-PRO-3, E-cadherin, and β -catenin in adult kidneys.

(B) Laminin whole-mount immunolabeling of the vastus (hindlimb muscle) of an adult mouse.

(C) PeCAM labeling in an E14.5 whole embryo. Partial projection of the chest region showing the heart, and detailed views of the whisker pad colabeled with TrkA. Anatomical abbreviations are listed in Table S4. Scale bars represent 500 μ m, except (A) lower row: 100 μ m.

See also Figures S2, S3, and S4, Tables S1, S2, S3, S4, and Movie S4.

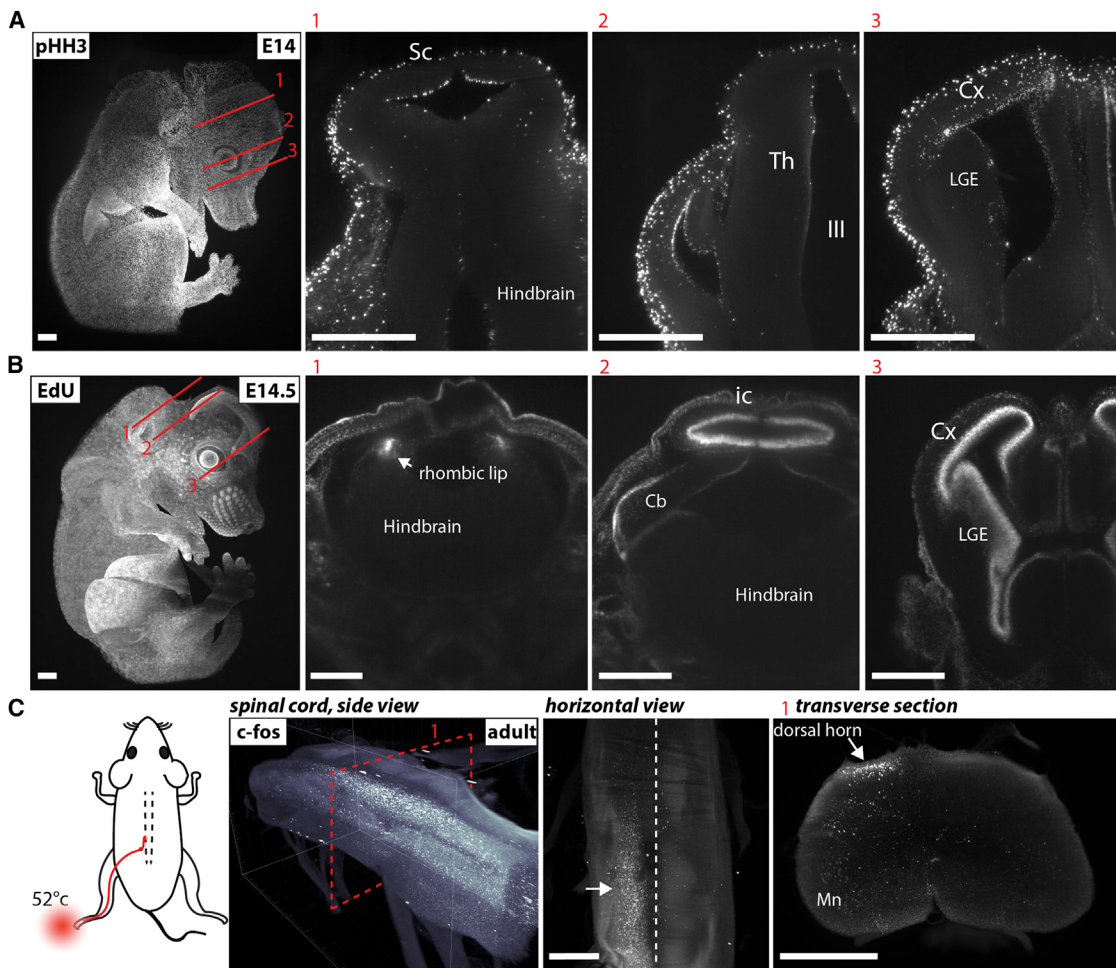


Figure 5. Application to Cell Proliferation and Neuronal Activity

(A) Whole-mount phosphohistone H3 immunolabeling of an E14 embryo, with details of mitotic cells in the midbrain (1), thalamus (2), or cortical ventricular zone (3).

(B) E14.5 embryo treated for 1 hr with an EdU pulse before fixation, showing proliferating cells in the skin and in diverse brain regions, such as the rhombic lips (arrowhead), cerebellum, and midbrain (2) and cortical ventricular zone (3).

(C) c-fos expression in the lumbar region of the spinal cord in an adult mouse after a heat stimulation of the hind paw. 3D view of the spinal cord, projection of horizontal planes, and optical section in the coronal plane. c-fos expression is seen on the side ipsilateral to the stimulation in the dorsal horn interneurons. Anatomical abbreviations are listed in Table S4. Scale bars represent 500 μ m.

See also Tables S1, S2, S3, and S4 and Movies S5 and S6.

with a caspase activity reporter in zebrafish retinal ganglion cell axons (Campbell and Okamoto, 2013). Our results support the model that local activation of Casp3 is important for developmental pruning of sensory axons.

An important application of volume imaging is to count the absolute number of objects more easily than from tissue sections. We quantified the number of cCasp3 positive cells in each DRG in embryos ranging from E12.5 to E16.5 (Figure 6C). We confirmed that the number of apoptotic cells peaks at E14.5 (White et al., 1998) and found that apoptotic cells were present between E11.5 and E16.5, a larger range than previously appreciated. No cCasp3 positive cells were observed at E10.5 (data not shown). Interestingly, we found significant variability in the number of apoptotic cells between left and right ganglia from

the same spinal cord segment, but when the total number of apoptotic cells in ganglia were integrated over spinal cord segments that innervate a shared target (e.g., cervical DRGs [C5–C8] subserving the forelimbs) or over the entire embryo (C2–S1), the numbers of apoptotic cells were strikingly similar between sides (Figures 6D and S5). This apparent homeostasis fits with the model that neuronal numbers are set by competition for limiting amounts of target-derived trophic factor, such that neurons within any given DRGs might capture more (or less) of the target-derived factor(s) but the total number subserving a particular target would be fixed by target size.

Retinal ganglion cells (RGCs) projections from the retina to the dorsolateral geniculate nucleus (dLGN) or superior colliculus (SC) provide another commonly used system for studying axon

targeting and pruning *in vivo*. They can be efficiently anterogradely labeled by intravitreous injection of cholera toxin beta (CTb) conjugated to Alexa Fluor 594 or 488 (Muir-Robinson et al., 2002). We used 3DISCO to clear an adult mouse brain after bilateral injection of CTb-A594 and CTb-A488. On the light-sheet microscope, it was possible to scan through the dLGN and observe ipsilateral and contralateral territories at high resolution (Figure 7A). Whereas classical tissue sections may provide higher resolution image for any given 2D plane, the advantage of volume imaging is to make it possible to investigate the entire projections in different orientations using a single sample.

One limitation of bulk CTb injections is the difficulty of resolving single axons and their terminals because of massive labeling. To observe single RGC axon projections with high resolution in adult brain using iDISCO, we sparsely labeled axons from RGCs with intravitreous injection of an adeno-associated virus (AAV2) driving expression of tdTomato. We immunolabeled the entire brain (cortex removed) using an antibody to RFP. Single axons labeled throughout the whole brain could be visualized from the optic nerve to the dLGN and SC (Figure 7B). To study neurodegeneration, we performed optic nerve crush injuries and observed degeneration of single axons in the brain. The transparency of the tissue was such that degenerated axons in the optic chiasm could be imaged from the dorsal side of the brain, through the entire tissue (Figure 7B). This method allows for a simple and rapid assessment of axon degeneration and regeneration in various regions of the central nervous system following different neural insults or under pathological conditions.

DISCUSSION

We have leveraged the 3DISCO clearing protocol to devise a rapid and simple yet powerful method, iDISCO, for whole-mount immunolabeling and 3D visualization of molecular markers in large, complex, intact embryonic, and adult tissues. The detailed iDISCO protocol can be found in the [Extended Experimental Procedures](#) and as a bench protocol available online ([Data S2](#)). Our experience is that for any given antibody, the quality of immunolabeling observed on tissue sections predicts the quality that will be observed with whole-mount immunolabeling using iDISCO, making the method very versatile. A number of important experimental considerations warrant discussion.

Choice of Tissue Clearing Protocol

Many clearing protocols have recently been published. They represent a valuable toolbox to address different questions, which may be best answered with different protocols. iDISCO is particularly powerful for immunolabeling applications. CLARITY or CUBIC may be better if the desired application is to image endogenous fluorescence of reporters such as GFP or tdTomato, which is quenched within 7–8 hours by the 3DISCO clearing procedure (Ertürk et al., 2014; Ke et al., 2013). In practice, however, this is not a serious limitation for iDISCO, because such reporters can also be visualized by immunolabeling them. In fact, it can often be more advantageous to visualize them by immunolabeling, as their endogenous fluorescence can fade during prolonged imaging and storage of archived samples,

whereas the Alexa Fluor dyes used in iDISCO are highly resistant to bleaching and stable in long-term storage at room temperature. As well, because of tissue autofluorescence in the blue-green spectrum (Figure S1), imaging of fluorescence from the most common reporters like GFP (that emit in that spectrum) is de facto limited to transgenic lines with high expression—the only examples reported so far in the literature. In contrast, with immunolabeling the signal from the transgenic reporter can be boosted and shifted to the far-red region of the spectrum to avoid tissue autofluorescence, enabling detection of moderately expressed reporters in addition to endogenous antigens.

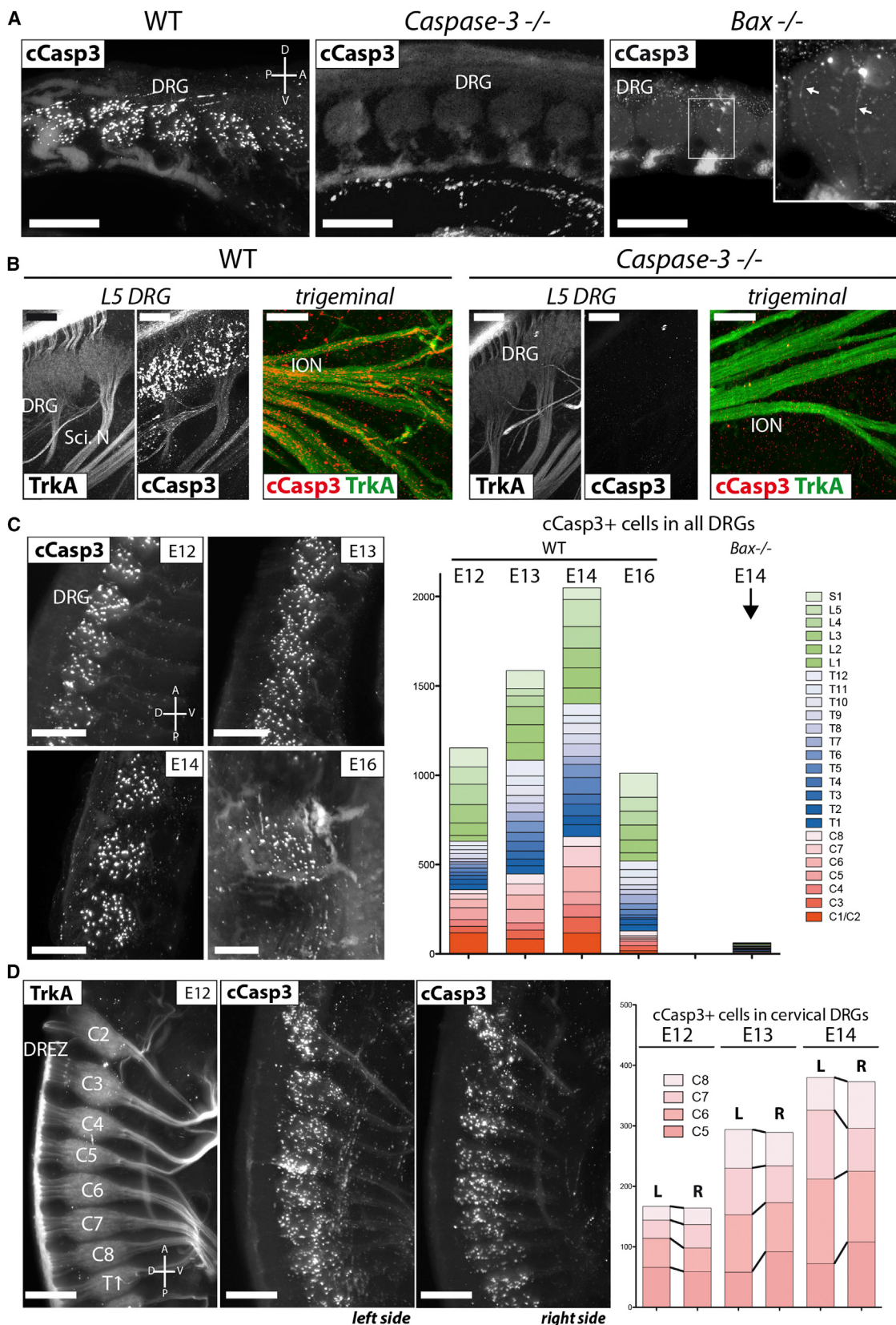
One limitation of iDISCO is that it is currently incompatible with the original Brainbow and Confetti mice (Livet et al., 2007; Snijper et al., 2010), which provide a rich spectral repertoire of fluorescent signals from multiple fluorescent proteins expressed simultaneously, because antibodies that distinguish those proteins are not available. However, the newer version 3 Brainbow lines have been designed to support immunostaining by use of non-cross-reacting antibodies to individual fluorescent proteins (Cai et al., 2013) and thus could be compatible with iDISCO.

Selection of Antibodies

All 28 antibodies used in this study gave good results with iDISCO (Table S3), but it should be noted that the antibodies were carefully prescreened. We first tested antibodies on sections pretreated with methanol to mimic the effect of methanol in the iDISCO protocol. Twenty-five of the antibodies gave good results in that test (Table S3) and all performed very well in iDISCO using methanol pretreatment (i.e., with similar signal-to-noise ratios as on sections). For the three antibodies whose epitopes were sensitive to methanol pretreatment (anti-PECAM, anti-cCasp9, and one of the anti-GFP antibodies; Table S3), iDISCO was performed with the no-methanol version of the protocol, which also gives good results (see Figure 4C for anti-PECAM staining) but can require longer incubation times and yield greater tissue autofluorescence (see below). Note also that the primary antibodies used here were all made in rabbits, goats, rats, or chickens (Table S3). We specifically avoided antibodies made in mice, as they often give high background on mouse tissues when detected with anti-mouse secondary antibodies. In line with that expectation, a pilot experiment with a mouse monoclonal antibody to Calbindin (Swant; no. 300) on adult brain yielded less satisfactory results (i.e., although there was a strong signal, there was also high background; data not shown). Further studies are required to determine whether the background is due to use of anti-mouse secondary antibody, and whether any background that is observed can be reduced by modifying the protocol.

Antibody Penetration

We achieved complete antibody diffusion in samples that are large enough that they are representative of most mouse samples of interest. We tested intact mouse embryos for stages up to E18, and found good penetration at all stages, and we verified that antibodies can label the center of intact adult mouse brains (undissected) with just 4 days of primary antibody incubation at 37°C. Nonetheless, to maximize antibody penetration in a reasonable time frame and to permit use of lower primary antibody concentrations, we recommend dissecting organs of



(legend on next page)

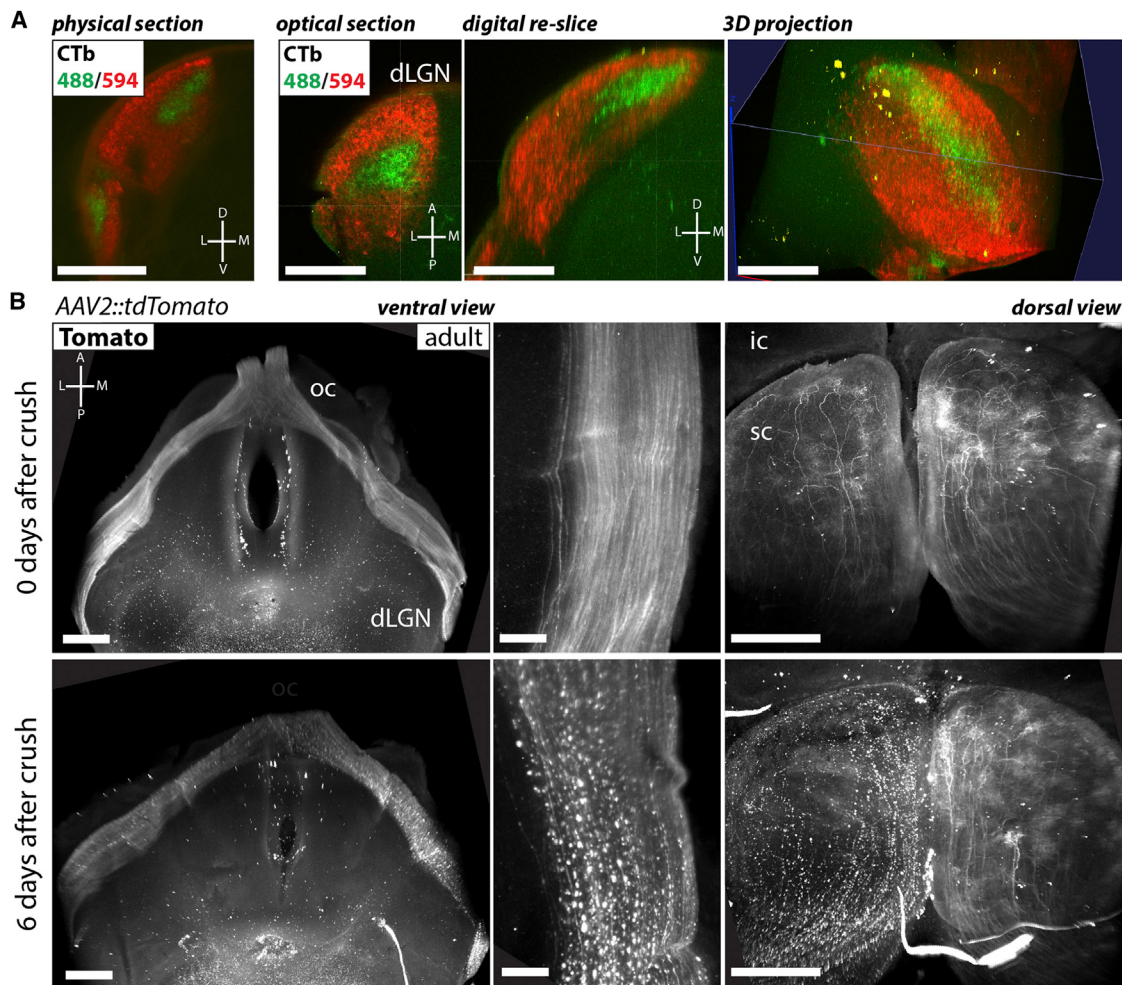


Figure 7. Study of Neurodegeneration with iDISCO

(A) Tracing of the visual projections in a 3-week-old mouse by cholera toxin beta (CTb) injection in the eye. Ipsilateral projections pseudocolored in green, contralateral in red. Coronal vibratome section (100 μ m) at the level of the dLGN nucleus (left panel) compared to a horizontal optical section and reconstructions in the coronal plane or in a 3D lateral view (right three panels).

(B) Adult wild-type mouse brain (cortices removed) labeled for tdTomato after a bilateral viral delivery of AAV2::tdTomato in the retina. The optic nerve was crushed unilaterally and the brain harvested after 0 or 6 days. Axon fragmentation can be seen 6 days after the nerve crush in the visual tracts and at the axons terminals in the superior colliculus. Anatomical abbreviations are listed in Table S4. Scale bars represent 500 μ m except optic tracts (100 μ m).

See also Tables S1, S2, S3, and S4.

interest from embryos older than E16, and in general we recommend trimming samples to a size relevant to the biological question. For example, in the case of adult brain, when compatible

with the study aims we have cut the forebrain in half sagittally or removed one or both cortices to achieve faster diffusion times and to maximize image quality.

Figure 6. Analysis of cCasp3 in Sensory Neurons and Their Axons

(A) Whole mount labeling of E14.5 wild-type, Caspase3^{-/-}, and Bax^{-/-} embryos for cCasp3. cCasp3 is abundantly detected in wild-type DRG neurons, but in much reduced levels in Bax^{-/-} embryos and not at all in Caspase3^{-/-} embryos. Inset in the Bax^{-/-} embryo shows individual cCasp3+ axons within a DRG (arrows).

(B) High-magnification view of the lumbar region and whisker pad, showing cCasp3 staining in sensory axons (double-labeled with TrkA) in wild-type and Caspase3^{-/-} embryos. Axonal cCasp3 is not detected in Caspase3^{-/-} embryos.

(C) Whole mount E12.5, E13.5, E14.5, and E16.5 embryos labeled for cCasp3. The number of cCasp3+ cells peaks at E14.5. The number is drastically reduced in the Bax^{-/-} at E14.

(D) View of the left and right sides of the same embryo at E12.5, and comparison of cCasp3 counts on both sides. Although the numbers of cCasp3 can change between cognate DRGs from the two sides, the overall sum remains the same for DRGs projecting to the same target regions. Anatomical abbreviations are listed in Table S4. Scale bars represent 500 μ m (A), 100 μ m (B) and 200 μ m (C and D).

See also Figure S5 and Tables S1, S2, S3, and S4.

Antibody concentration is an important factor that must be optimized to achieve good labeling. Our results indicate that antibody availability is not limiting for sparsely or moderately expressed proteins, such as transcription factors, subclass-specific markers, or reporter genes. For such antigens—the majority of those tested here—the very same antibody concentration used for IHC on tissue sections can also be used in the iDISCO procedure (Table S3). However, we also found that bioavailability of antibodies against proteins that are highly abundant and widely expressed, such as PeCAM, acetylated tubulin, or Aquaporin 2, can be more limited, presumably because of titration of available antibody molecules by the large amount of antigen present (Figure S2). We found that this problem can be overcome by reducing the size of the sample through trimming, by performing multiple rounds of antibody labeling at the regular concentration (although that extends the time needed for labeling), or by increasing antibody concentration (although that increases expense).

Finally, as mentioned, for antibodies compatible with methanol pretreatment, we recommend using the bleaching step to minimize background autofluorescence and to improve diffusion. Antibodies incompatible with methanol pretreatment worked well within our time frame on embryos and small adult tissues (e.g., a dissected cerebellum or 1 mm sections), but their diffusion was slower in large samples (e.g., whole adult brain).

Application to Different Tissues

We showed that iDISCO is useful across many organs, including kidney, muscle, stomach, and the vasculature. However, whether it is advantageous to use the protocol will depend on the application. Many tissues have highly repetitive structures that can already be well documented in sections. Tissue-specific protocols that add steps to preserve integrity of fragile tissues during collection and preparation have been developed, e.g., to study lung tissue (Scott et al., 2014) and adult skin (Li et al., 2011); some of these are likely compatible with iDISCO, but this needs to be tested. Similarly, bone can be immunolabeled in sections only after decalcification, but it is not yet known if that is compatible with iDISCO. Finally, during iDISCO tissues shrink slightly but consistently because of dehydration, so that absolute distance or volume measurements (to compare to live conditions) will require some kind of correction. However, tissue shrinkage does not change projection or connectivity patterns or relative distances, allowing detailed comparisons across different samples all treated by iDISCO.

Microscopy

It is important to choose the appropriate imaging setup. Scanning microscopes (confocal or two-photon) can achieve the best resolution throughout the whole imaging plane. However, the slow scanning speeds make them impractical for imaging large fields of view (Figure S3). Larger fields of view can be acquired by tiling, but lens distortions (pincushion or barrel distortions), light fall-off, and potential micromovements of the sample inside the chamber make it difficult to obtain good data sets. Light-sheet microscopy has more recently emerged as a good alternative to image large samples. The advantages of light-sheet microscopy over point-scanning microscopy are

reduced sample bleaching, high acquisition speed, large fields of view, and high dynamic range (Tomer et al., 2014). Its resolution can be more limited, but for many applications it provides a superior option, in particular for imaging large numbers of samples.

Data Processing

Volume imaging generates very large data sets, which can be challenging to manage. Modern light-sheet microscopes equipped with 5 megapixel sCMOS cameras produce image stacks of ~20 Gb for a scan spanning the entire working distance of the objective (6 mm). Most desktop computers are not able to open such data sets in RAM memory. However, one can conveniently open the stacks as “virtual stacks.” It is possible in this mode to perform maximum projections, or downsample the images to a more manageable size to perform 3D projections directly on ImageJ. However, more complex operations such as object tracing, automated counting and animated fly-overs are better done on proprietary software such as Biplane’s Imaris, and require a powerful workstation.

Implementation and Expense

iDISCO compares favorably with all other protocols in terms of ease of implementation. It is also inexpensive for sample preparation, clearing, and mounting for volume imaging. We do recommend use of a light-sheet microscope for fast volume imaging of large samples and of a high-end image workstation for processing large data sets, but the associated costs are similar for all volume imaging protocols.

In conclusion, we believe that iDISCO provides a versatile and reliable way to perform immunolabeling followed by volume imaging for a wide range of applications. Indeed, although preliminary tests are required to assess the best imaging parameters, antibody concentrations and incubation times, once those have been determined it becomes possible to use our workflow for large-scale screens.

EXPERIMENTAL PROCEDURES

Mice

All surgical and behavioral procedures in mice were performed in compliance with protocols approved by the Institutional Animal Care and Use Committee (IACUC) of the Rockefeller University. The Ai14 line (*Rosa26^{lox-stop-lox-dTomato}*), Thy1-GFPM, ChAT-cre, Caspase 3, and Bax mutant lines were obtained from the Jackson Laboratory. The *Netrin-1* gene-trap line was previously described (Serafini et al., 1996).

Sample Collection

The day of vaginal plug is defined as E0.5. Embryos were collected in ice-cold Leibovitz's L-15. Adult mice were heavily anesthetized with an overdose of isoflurane and fixed with an intracardiac perfusion of 4% PFA in PBS. All harvested samples were postfixed overnight at 4°C in 4% PFA in PBS, and then again 1 hr at room temperature the next day.

Sample Pretreatment with Methanol

Fixed samples were washed in PBS for 1 hr twice, then in 50% methanol (in PBS) for 1 hr, 80% methanol for 1 hr, 100% methanol for 1 hr twice. Samples were then bleached with 5% H₂O₂ in 20% DMSO/methanol (1 vol 30% H₂O₂/1 vol DMSO/4 vol methanol, ice cold) at 4°C overnight. After bleaching, samples were washed in methanol for 1 hr twice, then in 20% DMSO/methanol for 1 hr twice, then in 80% methanol for 1 hr, 50% methanol for 1 hr, PBS for 1 hr twice,

and finally in PBS/0.2% Triton X-100 for 1 hr twice before further staining procedures.

Sample Pretreatment without Methanol

Fixed samples were washed in PBS for 1 hr twice, then in PBS/0.2% Triton X-100 for 1 hr twice, then incubated in PBS/0.2% Triton X-100/20% DMSO at 37°C overnight, then in PBS/0.1% Tween-20/0.1% Triton X-100/0.1% deoxycholate/0.1% NP40/20% DMSO at 37°C overnight, then washed in PBS/0.2% Triton X-100 for 1 hr twice before further staining procedures.

EdU Labeling Protocol

EdU was suspended in 0.9% NaCl and injected at 50 mg/kg intraperitoneally (i.p.) 1 hr prior to tissue harvest. We used the click reaction-based EdU imaging kit (Invitrogen; MP10637) to label actively proliferating cells in embryos and adult organs.

Immunolabeling Protocol

Pretreated samples were incubated in PBS/0.2% Triton X-100/20% DMSO/0.3 M glycine at 37°C overnight, then blocked in PBS/0.2% Triton X-100/10% DMSO/6% Donkey Serum at 37°C for indicated time (Table S2). Samples were washed in PBS/0.2% Tween-20 with 10 µg/ml heparin (PTwH) for 1 hr twice, then incubated in primary antibody dilutions in PTwH/5% DMSO/3% Donkey Serum at 37°C for indicated time. Samples were then washed in PTwH for 1 day, then incubated in secondary antibody dilutions in PTwH/3% Donkey Serum at 37°C for indicated time. Samples were finally washed in PTwH for 2 days before clearing and imaging. For nuclear labeling, immunolabeled samples were incubated with TO-PRO-3 (1:5,000 in PTwH) for 1 hr, then washed in PTwH.

Tissue Clearing and Precautions with Solvents

Immunolabeled or traced tissues were cleared with a simplified version of 3DISCO (Ertürk et al., 2012a). Samples were incubated overnight in 10 ml of 50% v/v tetrahydrofuran/H₂O (THF) (Sigma 186562-12X100ML). Samples were then incubated for 1 hr in 10 ml of 80% THF/H₂O and twice 1 hr in 100% THF and then in dichloromethane (DCM) (Sigma 270997-12X100ML) until they sank at the bottom of the vial. Finally, samples were incubated in 18 ml of dibenzyl ether (DBE) (Sigma 108014-1KG) until clear (~2 hr) and then stored in DBE at room temperature. Organic solvents should be handled under a chemical hood and disposed of following local health and safety regulations. DBE, which is used for storage and imaging, is a skin irritant exhibiting toxicity class II (moderate toxicity) according to the material safety data sheets (MSDSs) and should be handled with care, including wearing gloves, but with those precautions can be used on an open bench for slide mounting and for microscopy.

Imaging

Large samples (embryos from E12.5 and dissected organs) were imaged on a light-sheet microscope (Ultramicroscope II, LaVision Biotec) equipped with a sCMOS camera (Andor Neo) and a 2×/0.5 objective lens equipped with a 6 mm working distance dipping cap. Samples presented in Figure 2C (E16 Forearm), Figure 3B (cortical neurons), Figure 6B (DRGs and trigeminal nerve), and Figure 7A (dLGN) were imaged on a 2 photon microscope (Olympus) with a 10×/0.6, 3 mm working distance or a 25×/1.05, 2 mm working distance objective.

Image Processing and Analysis

Because of the very high dynamic range (15 bit) of the images generated on the light sheet microscope, for display purposes a gamma correction was applied on data sets obtained from the light-sheet microscope. Maximum projections were performed using ImageJ (NIH, <http://imagej.nih.gov/ij/>). Simple 3D projections were performed with VAA3D (Peng et al., 2010) on desktop-class computers. Imaris (Bitplane, <http://www.bitplane.com/imaris/imaris>) was used for 3D manipulations. cCasp3+ cells were counted from maximum projections encompassing the entire DRGs and the data where plotted with Prism (Graphpad, <http://www.graphpad.com/scientific-software/prism/>).

Cholera Toxin Beta Eye Injection

Animals were anesthetized with isoflurane. One microliter of 1% cholera toxin in PBS conjugated to either Alexa Fluor 594 or Alexa Fluor 488 was injected into the retina with a fine Hamilton Syringe. Mice were analyzed after 24 hr. After fixation by cardiac perfusion with 4% paraformaldehyde in PBS, brains were dissected and postfixed in 4% PFA in PBS overnight at 4°C. Brains were then washed in PBS for 1 hr at room temperature, cleared, and imaged.

Nerve Injuries

For sciatic nerve crush, the mice were anesthetized, an incision was made between the knee and the hip joint, and the gluteal muscles were separated. The sciatic nerve was crushed for 30 s with a pair of fine forceps. Twenty-four hours after nerve injury the mice were perfused, and L4 and L5 DRGs were dissected and postfixed overnight at 4°C. For optic nerve crush, intravitreal injection of AAV2 was performed on 2- to 4-month-old animals. For sparse labeling, 2 × 10³ transduction units of AAV2 were delivered. Three weeks after viral injection, mice were anesthetized, and topical antibiotic ointment was applied to the eyes before optic nerve crush surgery. An incision was made on the superior conjunctiva of the left eye, and the optic nerve was exposed by a pair of blunt forceps. The crush injury was performed for 10 s using a pair of fine-tip forceps at ~1 mm distal from the eyeball.

Heat Stimulation for c-fos Expression Induction

One-month-old C57Bl/6 mice were anesthetized with isoflurane and their left paws were dipped ten times for 5 s each in a water bath at 52°C (10 s intervals between each stimulation). Mice were returned to their cage for 2 hr then anesthetized with an overdose of isoflurane and perfused with 4% PFA in PBS.

SUPPLEMENTAL INFORMATION

Supplemental Information includes Extended Experimental Procedures, five figures, two data files, four tables, and six movies and can be found with this article online at <http://dx.doi.org/10.1016/j.cell.2014.10.010>.

AUTHOR CONTRIBUTIONS

N.R., Z.W., D.S., and M.T.-L. designed the study. N.R., Z.W., D.S., P.A., and M.T.-L. wrote the paper. N.R., Z.W., D.S., and J.Y. performed the experiments. P.A. designed the 3D-printed chambers and helped with imaging of samples.

ACKNOWLEDGMENTS

We thank Frank Bradke and Alain Chédotal for sharing insights on 3DISCO, Olav Olsen for valuable input, Ricardo Azevedo for technical support, and other members of the M.T.-L. laboratory for helpful discussions. Our gratitude goes to other team members of the Rockefeller University Bio-Imaging Resource Center, and in particular Kaye Thomas, Tao Tong, and Alison North. Supported by The Rockefeller University. N.R. is supported by an EMBO long-term fellowship. The imaging center is supported by the Empire State Stem Cell Fund through New York State Department of Health (NYSDOH) contract C023046. Opinions expressed here are solely those of the author and do not necessarily reflect those of the Empire State Stem Cell Fund, the NYSDOH, or the state of NY.

Received: June 12, 2014

Revised: July 29, 2014

Accepted: October 2, 2014

Published: October 30, 2014

REFERENCES

- Abraira, V.E., and Ginty, D.D. (2013). The sensory neurons of touch. *Neuron* 79, 618–639.
Cai, D., Cohen, K.B., Luo, T., Lichtman, J.W., and Sanes, J.R. (2013). Improved tools for the Brainbow toolbox. *Nat. Methods* 10, 540–547.

- Campbell, D.S., and Okamoto, H. (2013). Local caspase activation interacts with Slit-Robo signaling to restrict axonal arborization. *J. Cell Biol.* 203, 657–672.
- Chung, K., Wallace, J., Kim, S.-Y., Kalyanasundaram, S., Andelman, A.S., Davidson, T.J., Mirzabekov, J.J., Zalocusky, K.A., Mattis, J., Denisin, A.K., et al. (2013). Structural and molecular interrogation of intact biological systems. *Nature* 497, 332–337.
- Deckwerth, T.L., Elliott, J.L., Knudson, C.M., Johnson, E.M., Jr., Snider, W.D., and Korsmeyer, S.J. (1996). BAX is required for neuronal death after trophic factor deprivation and during development. *Neuron* 17, 401–411.
- Dodt, H.-U., Leischner, U., Schierloh, A., Jährling, N., Mauch, C.P., Deininger, K., Deussing, J.M., Eder, M., Ziegglänsberger, W., and Becker, K. (2007). Ultramicroscopy: three-dimensional visualization of neuronal networks in the whole mouse brain. *Nat. Methods* 4, 331–336.
- Enard, W., Gehre, S., Hammerschmidt, K., Höltner, S.M., Blass, T., Somel, M., Brückner, M.K., Schreweis, C., Winter, C., Sohr, R., et al. (2009). A humanized version of Foxp2 affects cortico-basal ganglia circuits in mice. *Cell* 137, 961–971.
- Ertürk, A., Becker, K., Jährling, N., Mauch, C.P., Hojer, C.D., Egen, J.G., Hellal, F., Bradke, F., Sheng, M., and Dodt, H.U. (2012a). Three-dimensional imaging of solvent-cleared organs using 3DISCO. *Nat. Protoc.* 7, 1983–1995.
- Ertürk, A., Mauch, C.P., Hellal, F., Förstner, F., Keck, T., Becker, K., Jährling, N., Steffens, H., Richter, M., Hübener, M., et al. (2012b). Three-dimensional imaging of the unsectioned adult spinal cord to assess axon regeneration and glial responses after injury. *Nat. Med.* 18, 166–171.
- Ertürk, A., Lafkas, D., and Chalouni, C. (2014). Imaging cleared intact biological systems at a cellular level by 3DISCO. *J. Vis. Exp.* Published online July 7, 2014. <http://dx.doi.org/10.3791/51382>.
- Feng, G., Mellor, R.H., Bernstein, M., Keller-Peck, C., Nguyen, Q.T., Wallace, M., Nerbonne, J.M., Lichtman, J.W., and Sanes, J.R. (2000). Imaging neuronal subsets in transgenic mice expressing multiple spectral variants of GFP. *Neuron* 28, 41–51.
- Ferland, R.J., Cherry, T.J., Prewar, P.O., Morrisey, E.E., and Walsh, C.A. (2003). Characterization of Foxp2 and Foxp1 mRNA and protein in the developing and mature brain. *J. Comp. Neurol.* 460, 266–279.
- Frederic, F., Hainaut, F., Thomasset, M., Guenet, J.L., Delhaye-Bouchaud, N., and Mariani, J. (1992). Cell counts of Purkinje and inferior olfactory neurons in the 'hyperspiny Purkinje cells' mutant mouse. *Eur. J. Neurosci.* 4, 127–135.
- Fujita, H., and Sugihara, I. (2012). FoxP2 expression in the cerebellum and inferior olive: development of the transverse stripe-shaped expression pattern in the mouse cerebellar cortex. *J. Comp. Neurol.* 520, 656–677.
- Goelet, P., Castellucci, V.F., Schacher, S., and Kandel, E.R. (1986). The long and the short of long-term memory—a molecular framework. *Nature* 322, 419–422.
- Hama, H., Kurokawa, H., Kawano, H., Ando, R., Shimogori, T., Noda, H., Fukami, K., Sakaue-Sawano, A., and Miyawaki, A. (2011). Scale: a chemical approach for fluorescence imaging and reconstruction of transparent mouse brain. *Nat. Neurosci.* 14, 1481–1488.
- Horng, S., Kreiman, G., Ellsworth, C., Page, D., Blank, M., Millen, K., and Sur, M. (2009). Differential gene expression in the developing lateral geniculate nucleus and medial geniculate nucleus reveals novel roles for Zic4 and Foxp2 in visual and auditory pathway development. *J. Neurosci.* 29, 13672–13683.
- Hunt, S.P., Pini, A., and Evan, G. (1987). Induction of c-fos-like protein in spinal cord neurons following sensory stimulation. *Nature* 328, 632–634.
- Ke, M.-T., Fujimoto, S., and Imai, T. (2013). SeeDB: a simple and morphology-preserving optical clearing agent for neuronal circuit reconstruction. *Nat. Neurosci.* 16, 1154–1161.
- Kuwajima, T., Sitko, A.A., Bhansali, P., Jurgens, C., Guido, W., and Mason, C. (2013). ClearT: a detergent- and solvent-free clearing method for neuronal and non-neuronal tissue. *Development* 140, 1364–1368.
- Li, L., Rutlin, M., Abraira, V.E., Cassidy, C., Kus, L., Gong, S., Jankowski, M.P., Luo, W., Heintz, N., Koerber, H.R., et al. (2011). The functional organization of cutaneous low-threshold mechanosensory neurons. *Cell* 147, 1615–1627.
- Lindsten, T., Ross, A.J., King, A., Zong, W.X., Rathmell, J.C., Shiels, H.A., Ulrich, E., Waymire, K.G., Maher, P., Frauwrith, K., et al. (2000). The combined functions of proapoptotic Bcl-2 family members Bak and Bax are essential for normal development of multiple tissues. *Mol. Cell* 6, 1389–1399.
- Livet, J., Weissman, T.A., Kang, H., Draft, R.W., Lu, J., Bennis, R.A., Sanes, J.R., and Lichtman, J.W. (2007). Transgenic strategies for combinatorial expression of fluorescent proteins in the nervous system. *Nature* 450, 56–62.
- Middleton, G., and Davies, A.M. (2001). Populations of NGF-dependent neurons differ in their requirement for BAX to undergo apoptosis in the absence of NGF/TrkA signalling in vivo. *Development* 128, 4715–4728.
- Muir-Robinson, G., Hwang, B.J., and Feller, M.B. (2002). Retinogeniculate axons undergo eye-specific segregation in the absence of eye-specific layers. *J. Neurosci.* 22, 5259–5264.
- Oh, W.-J., and Gu, C. (2013). Establishment of neurovascular congruity in the mouse whisker system by an independent patterning mechanism. *Neuron* 80, 458–469.
- Peng, H., Ruan, Z., Long, F., Simpson, J.H., and Myers, E.W. (2010). V3D enables real-time 3D visualization and quantitative analysis of large-scale biological image data sets. *Nat. Biotechnol.* 28, 348–353.
- Reginensi, A., Scott, R.P., Gregorieff, A., Bagherie-Lachidan, M., Chung, C., Lim, D.-S., Pawson, T., Wrana, J., and McNeill, H. (2013). Yap- and Cdc42-dependent nephrogenesis and morphogenesis during mouse kidney development. *PLoS Genet.* 9, e1003380.
- Scott, G.D., Blum, E.D., Fryer, A.D., and Jacoby, D.B. (2014). Tissue optical clearing, three-dimensional imaging, and computer morphometry in whole mouse lungs and human airways. *Am. J. Respir. Cell Mol. Biol.* 51, 43–55.
- Serafini, T., Colamarino, S.A., Leonardo, E.D., Wang, H., Bedington, R., Skarnes, W.C., and Tessier-Lavigne, M. (1996). Netrin-1 is required for commissural axon guidance in the developing vertebrate nervous system. *Cell* 87, 1001–1014.
- Simon, D.J., Weimer, R.M., McLaughlin, T., Kallop, D., Stanger, K., Yang, J., O'Leary, D.D.M., Hannoush, R.N., and Tessier-Lavigne, M. (2012). A caspase cascade regulating developmental axon degeneration. *J. Neurosci.* 32, 17540–17553.
- Snippert, H.J., van der Flier, L.G., Sato, T., van Es, J.H., van den Born, M., Kroon-Veenboer, C., Barker, N., Klein, A.M., van Rheenen, J., Simons, B.D., and Clevers, H. (2010). Intestinal crypt homeostasis results from neutral competition between symmetrically dividing Lgr5 stem cells. *Cell* 143, 134–144.
- Spalteholz, W. (1914). Über das Durchsichtigmachen von menschlichen und tierischen Präparaten und seine theoretischen Bedingungen, nebst Anhang: Über Knochenfärbung (Leipzig: S. Hirzel).
- Sun, W., Gould, T.W., Vinsant, S., Prevette, D., and Oppenheim, R.W. (2003). Neuromuscular development after the prevention of naturally occurring neuronal death by Bax deletion. *J. Neurosci.* 23, 7298–7310.
- Susaki, E.A., Tainaka, K., Perrin, D., Kishino, F., Tawara, T., Watanabe, T.M., Yokoyama, C., Onoe, H., Eguchi, M., Yamaguchi, S., et al. (2014). Whole-brain imaging with single-cell resolution using chemical cocktails and computational analysis. *Cell* 157, 726–739.
- Tomer, R., Ye, L., Hsueh, B., and Deisseroth, K. (2014). Advanced CLARITY for rapid and high-resolution imaging of intact tissues. *Nat. Protoc.* 9, 1682–1697.
- White, F.A., Keller-Peck, C.R., Knudson, C.M., Korsmeyer, S.J., and Snider, W.D. (1998). Widespread elimination of naturally occurring neuronal death in Bax-deficient mice. *J. Neurosci.* 18, 1428–1439.
- Yang, B., Treweek, J.B., Kulkarni, R.P., Deverman, B.E., Chen, C.-K., Lubeck, E., Shah, S., Cai, L., and Gradinariu, V. (2014). Single-cell phenotyping within transparent intact tissue through whole-body clearing. *Cell* 158, 945–958.